Sensitivity Analysis of a RFRFR Continuum Parallel Robot

Luis Fernando Maldonado Saavedra, Quentin Peyron, Sébastien Briot, and Christian Duriez

Abstract The model of Continuum Parallel Robots (CPRs) often relies on an accurate knowledge of the material and geometrical properties of the system, which can be subjected to variations due to multiple factors such as fabrication parameters, oversimplifying assumptions, material fatigue, etc. This paper proposes a method based on a sensitivity analysis framework, that allows to map variations in the model parameters of a CPR to variations in the position of its End-Effector. Simulations of a planar RFRFR CPR, making use of the strong form of the Cosserat Rod model, are used to validate the method.

1 Introduction

Continuum Parallel Robots (CPRs) have been the subject of growing research interest because of their ability to combine the compactness, simplicity and compliance of Continuum Robots with the precision and strength of parallel architectures [3]. Their performance is usually evaluated using Jacobian based metrics, which focus on the behavior of the robot's End-Effector (EE). Such indicators can be used to quantify the robot's manipulability [3], analyze its

L. F. Maldonado Saavedra
Centre INRIA de l'Université de Lille, Villeneuve d'Ascq, France
e-mail: `luis-fernando.maldonado-saavedra@inria.fr`

Q. Peyron
Centre INRIA de l'Université de Lille, Villeneuve d'Ascq, France

S. Briot
Laboratoire des Sciences du Numérique de Nantes (LS2N), UMR CNRS 6004, Nantes France

C. Duriez
Centre INRIA de l'Université de Lille, Villeneuve d'Ascq, France

behavior near singular configurations [4], evaluate the stability of the obtained solution [8], and characterize a variety of additional behaviors. However, these indicators rely on an accurate knowledge of the model parameters, which can be subjected to uncertainties.

Indeed, CPRs often make use of polymers and elastomers produced by a series of chemical and physical processes such as silicone molding or 3D printing. Fabrication parameters including temperature, elastomer to curing agent ratio, and infill orientation can produce material properties that considerably differ from the ones found in literature [5, 9]. Additionally, the model of the material can be subjected to oversimplifying assumptions (isotropy, linear-elasticity, etc.), and materials can degrade over time or when exposed to a harsh environment. Furthermore, geometrical parameters such as the lengths of the different flexible segments, can also be subjected to variation due to fatigue and wear of the material [7]. Thus, there is a need to quantify the effect of variability of the parameters in a CPR model.

In this paper, we present a method to quantify how uncertainty in the model parameters of a CPR affects the position of its EE platform, by conducting a sensitivity analysis adapted from the works of Afifi et al. [1], and Srour [6], dedicated to the robust trajectory planning of drones.

Section 2 presents a brief summary of the modeling of CPRs making use of the Cosserat rod theory [3], as well as the necessary theoretical elements to carry out the sensitivity analysis and Section 3 aims to validate the method by performing simulations of a $\underline{\text{R}}$FRF$\underline{\text{R}}$ CPR.

2 Problem Formulation

2.1 Geometrico-static Model of CPRs

A CPR is composed of n flexible segments assembled in parallel. The shape of the i^{th} segment can be modeled by the Cosserat rod ordinary differential equations (ODE) in which a deformable body is represented as a set of a continuous rigid cross-sections stacked along the neutral fiber of the rod. Each cross-section is parametrized by its position $\boldsymbol{p}_i(s_i) \in \mathbb{R}^3$ and orientation in the form of a rotation matrix $\boldsymbol{R}_i(s_i) \in \text{SO}(3)$, forming a body reference frame which is a function of the arc length $s_i \in [0, l_i]$:

$$\boldsymbol{g}_i(s_i) = \begin{bmatrix} \boldsymbol{R}_i(s_i) & \boldsymbol{p}_i(s_i) \\ \emptyset_{1\times 3} & 1 \end{bmatrix} \in \text{SE}(3) \tag{1}$$

where SO(3) and SE(3) refer to the 3D special orthogonal and Euclidean groups, respectively. For the sake of space, in this paper we do not give details about the formulation of the Cosserat rod equations, the reader can refer to [3] for details.

Let the model of the i^{th}-leg be written as a generalized system of ODEs:

$$\boldsymbol{x}_i'(s_i) = \boldsymbol{f}_i(\boldsymbol{x}_i(s_i), \boldsymbol{\rho}_i) \quad \forall i \in 1, \dots, n \tag{2}$$

where $\boldsymbol{x}_i = [\boldsymbol{g}_i, \boldsymbol{n}_i, \boldsymbol{m}_i] \in \mathrm{SE}(3) \times \mathbb{R}^6$ is the state vector of the i^{th}-leg, composed of $\boldsymbol{g}_i$ the pose of the cross-section at s_i, $\boldsymbol{n}_i$ and $\boldsymbol{m}_i$, the internal force and moments of the leg, respectively. The symbol $(\cdot)'$ denotes the derivative with relation to the arc-length s_i, i.e. $\boldsymbol{x}_i'(s_i) = \frac{d\boldsymbol{x}_i(s_i)}{ds_i}$. Additionally, $\boldsymbol{\rho}_i \in \mathbb{R}^{n_{\rho_i}}$, denotes the vector of model parameters, composed of the mechanical properties of the material as well as geometrical parameters of the legs. Note that the parameters that appear in $\boldsymbol{\rho}_i$ can vary depending on the model formulation.

To form the model of a CPR, the single leg model in (2) is coupled with constraint equations issued from a static equilibrium of the EE platform and geometric constraints specific to the robot design. As presented in [3], the static equilibrium conditions can be written as follows:

$$\begin{cases} \sum_{i=1}^{n} [\boldsymbol{n}_i(l_i)] + \boldsymbol{f}_{\mathrm{P}} = \boldsymbol{0} \\ \sum_{i=1}^{n} [\boldsymbol{p}_i(l_i) \times \boldsymbol{n}_i(l_i)] - \boldsymbol{p}_{\mathrm{P}} \times \boldsymbol{f}_{\mathrm{P}} - \boldsymbol{m}_{\mathrm{P}} = \boldsymbol{0} \end{cases} \tag{3}$$

where $\boldsymbol{f}_{\mathrm{P}}$ and $\boldsymbol{m}_{\mathrm{P}}$ denote the external force and moment vectors applied at $\boldsymbol{p}_{\mathrm{P}}$, the center of the EE platform. The geometric constraints are based on the joint types that link the different flexible segments with the platform, and as such they vary according to the CPR design [3]. Here the geometric constraints are assembled into a vector equation taking the generic form:

$$\boldsymbol{\Psi}(\boldsymbol{q}_{\mathrm{P}}, \boldsymbol{g}_1(l_1), \dots, \boldsymbol{g}_n(l_n)) = 0 \tag{4}$$

Thus, the geometrico-static model of a CPR is formed by combining the constraints in (4), computed thanks to the integration of the Cosserat ODEs in (2), with a linear function allowing to fix either the motor positions or the EE configuration, represented by vectors $\boldsymbol{q}_a$ and $\boldsymbol{q}_{\mathrm{P}}$ respectively. i.e. either $\boldsymbol{q}_a - \boldsymbol{q}_a^d$ or $\boldsymbol{q}_{\mathrm{P}} - \boldsymbol{q}_{\mathrm{P}}^d$ with the superscript d indicating a set of variables imposed by the user.

The static configuration of the CPR is then obtained by canceling a residual taking the generic form:

$$\boldsymbol{\mathcal{R}}(\boldsymbol{y}, \boldsymbol{\rho}) = 0 \tag{5}$$

where $\boldsymbol{y} = [\boldsymbol{q}_a, \boldsymbol{q}_{\mathrm{P}}, \boldsymbol{\mu}]^T \in \mathbb{R}^{n_y}$ is the state vector of the robot, composed of $\boldsymbol{q}_a$ the actuation variables, $\boldsymbol{q}_{\mathrm{P}}$ the variables related to the pose of the EE platform and $\boldsymbol{\mu}$ the wrenches at the base of the different flexible segments, containing all variables $\boldsymbol{n}_i$ and $\boldsymbol{m}_i$ of the state vector $\boldsymbol{x}_i$ given below (2). Additionally, $\boldsymbol{\rho} = [\boldsymbol{\rho}_1, \dots, \boldsymbol{\rho}_n]^T \in \mathbb{R}^{n_\rho}$ denotes the vector of the robot parameters, obtained by concatenating the parameters vector of each segment.

2.2 Sensitivity Analysis Framework Applied to CPRs

The presented method is derived from the works in [1, 6], in which the sensitivity metrics are computed by forward integration along a time-dependent trajectory representing the motion of a mobile robot. In our case, these metrics are computed by integrating along a space curves, representing the robot's flexible legs. Despite the change in perspective, the equations can be solved in the same manner as in the previously cited works.

Each component ρ_{ij} of the parameters vector of each leg, $\boldsymbol{\rho}_i$, is assumed to lie inside a known range centered at a nominal value ρ_{ij}^*:

$$\rho_{ij} \in \left[\rho_{ij}^* - \delta\rho_{ij}, \rho_{ij}^* + \delta\rho_{ij}\right] \quad \begin{array}{l} \forall i = 1, \ldots, n \\ \forall j = 1, \ldots, n_{\rho_i} \end{array} \tag{6}$$

The leg's state sensitivity, noted $\boldsymbol{\Pi}_i(s_i)$, is defined as a matrix that quantifies how variations of the parameters $\boldsymbol{\rho}_i$ around their nominal values $\boldsymbol{\rho}_i^*$ will affect the evolution of the state $\boldsymbol{x}_i$ of the leg:

$$\boldsymbol{\Pi}_i(s_i) = \left.\frac{\partial \boldsymbol{x}_i(s_i)}{\partial \boldsymbol{\rho}_i}\right|_{\boldsymbol{\rho}_i = \boldsymbol{\rho}_i^*} \in \mathbb{R}^{n_{x_i} \times n_{\rho_i}} \tag{7}$$

This matrix generally cannot be computed in a closed form, but it can be obtained via forward integration of a differential equation along the curve:

$$\boldsymbol{\Pi}_i'(s_i) = \frac{\partial \boldsymbol{f}_i}{\partial \boldsymbol{x}_i}.\boldsymbol{\Pi}_i(s_i) + \frac{\partial \boldsymbol{f}_i}{\partial \boldsymbol{\rho}_i} \quad \text{with: } \boldsymbol{\Pi}_i(0) = 0 \tag{8}$$

The Jacobian matrices $\frac{\partial \boldsymbol{f}_i}{\partial \boldsymbol{x}_i}$ and $\frac{\partial \boldsymbol{f}_i}{\partial \boldsymbol{\rho}_i}$ are computed analytically in this paper, in general cases they can be obtained by numerical methods such as the finite difference method. The matrix $\boldsymbol{\Pi}_i(s_i)$ can then be used to compute different sensitivity metrics as presented in [1, 6].

In the case of the complete CPR, the full state sensitivity of the robot is defined as follows:

$$\boldsymbol{\Pi}_y = \left.\frac{\partial \boldsymbol{y}}{\partial \boldsymbol{\rho}}\right|_{\boldsymbol{\rho} = \boldsymbol{\rho}^*} \in \mathbb{R}^{n_y \times n_\rho} \tag{9}$$

This matrix is obtained by applying the implicit functions theorem to the residual in (5). Let $\boldsymbol{\mathcal{R}}(\boldsymbol{y}(\boldsymbol{\rho}), \boldsymbol{\rho}) = 0$, if $\frac{\partial \boldsymbol{\mathcal{R}}}{\partial \boldsymbol{y}}$ is invertible at a given point $[\boldsymbol{y}, \boldsymbol{\rho}]$, then:

$$\boldsymbol{\Pi}_y = -\frac{\partial \boldsymbol{\mathcal{R}}}{\partial \boldsymbol{\rho}}.\left(\frac{\partial \boldsymbol{\mathcal{R}}}{\partial \boldsymbol{y}}\right)^{-1} \tag{10}$$

In our application we can determine the analytical expression of the Jacobian matrices. With $\frac{\partial \boldsymbol{\mathcal{R}}}{\partial \boldsymbol{y}}$ making use of the transition matrix of the ODE of each leg and $\frac{\partial \boldsymbol{\mathcal{R}}}{\partial \boldsymbol{\rho}}$ making use of the state sensitivity matrices of each leg evaluated at their tip, $\boldsymbol{\Pi}_i(s_i = l_i)$. In a general case, these matrices can be numerically computed.

The full sensitivity matrix $\boldsymbol{\Pi}_y$ allows us to exploit ellipsoids to map variations in the parameter space to the state space of the system, assuming that the parameters in $\boldsymbol{\rho}$ belong to a bounded interval as seen in (6). For details about the computation of the ellipsoids, see [1, 6]. First, let us consider that the uncertain parameters lie inside an ellipsoid centered at $\boldsymbol{\rho}^*$, described by the equation:

$$\Delta\boldsymbol{\rho}^T.\boldsymbol{W}^{-1}.\Delta\boldsymbol{\rho} \leq 1 \tag{11}$$

with $\Delta\boldsymbol{\rho} = \boldsymbol{\rho} - \boldsymbol{\rho}^*$, the variation of the parameters around their nominal value, and $\boldsymbol{W} = \mathrm{diag}(\delta\rho_{ij}^2) \in \mathbb{R}^{n_\rho \times n_\rho}$ a weights' matrix used to scale the different parameters by their corresponding variation range as presented in (6). Assuming, $\Delta\boldsymbol{\rho}$ is sufficiently small, (9) can be written as:

$$\Delta\boldsymbol{y} \approx \boldsymbol{\Pi}_y.\Delta\boldsymbol{\rho} \tag{12}$$

with $\Delta\boldsymbol{y} = \boldsymbol{y} - \boldsymbol{y}^*$, where $\boldsymbol{y}^*$ is the state that satisfies (5) in the nominal case. Equation (11) can then be rewritten to define the uncertainty ellipsoid in the state space:

$$\begin{aligned} \Delta\boldsymbol{y}^T.\left(\boldsymbol{\Pi}_y\boldsymbol{W}\boldsymbol{\Pi}_y^T\right)^{-1}\Delta\boldsymbol{y} \leq 1 \\ \Delta\boldsymbol{y}^T\boldsymbol{K}_{\boldsymbol{\Pi}_y}^{-1}\Delta\boldsymbol{y} \leq 1 \end{aligned} \tag{13}$$

with $\boldsymbol{K}_{\boldsymbol{\Pi}_y} = \boldsymbol{\Pi}_y\boldsymbol{W}\boldsymbol{\Pi}_y^T$ a symmetric and positive semi-definite matrix called the state sensitivity kernel matrix.

As such, when the parameters $\boldsymbol{\rho}$ vary inside the ellipsoid defined by (11), the corresponding perturbed state $\boldsymbol{y}$ will be located inside the ellipsoid in (13). These equations are based in the first order approximation given in (12). Despite this approximation, the method yields satisfactory results, as it will be shown in the next section.

3 Case Study: Planar RFRFR CPR with 4 Parameters

As presented by Altuzarra et al. in [2], the planar RFRFR CPR is composed of two flexible segments linked by a pivot joint at their extremities and actuated by revolute motors at their bases. Additionally, as seen in Figure 1, the model in [2] is modified to also take into account the rigid segments that connect the legs to the motors and to the pivot joint as well as the pre-curvature of the rods at rest. The legs are modeled using a simplified version of the Cosserat rod model in which the segment is considered to be inextensible and unshearable (Kirchhoff assumptions), and only bending stresses in the yz-plane are taken into account.

Let $\boldsymbol{\xi}_i = [p_{yi}, p_{zi}, \theta_i]^T$ represent the position and orientation of the cross-section at arc-length s_i for the i^{th} rod. Let $\boldsymbol{\mu}_i = [n_{yi}, n_{zi}, m_{xi}]^T$ denote the internal forces and moments of the rod, and let $\boldsymbol{w}_{\text{ext}} = [f_{yi}, f_{zi}, l_{xi}]^T$ be the external distributed forces and moments applied at the rod. By dropping the dependency of s_i for the sake of space, the geometrico-static model of the rod in the yz-plane, can be written as follows:

$$\forall i = 1,2 \quad \begin{cases} \boldsymbol{\xi}_i' = \begin{bmatrix} \cos\theta_i \\ \sin\theta_i \\ \frac{m_{xi}}{k_{bi}} + \frac{1}{r_{ci}} \end{bmatrix} \\ \boldsymbol{\mu}_i' = \begin{bmatrix} -f_{yi} \\ -f_{zi} \\ n_{yi}.\sin\theta_i - n_{zi}\cos\theta_i - l_{xi} \end{bmatrix} \\ \text{with:} \quad \boldsymbol{\xi}_i(0) = \boldsymbol{\xi}_{i0}, \ \boldsymbol{\mu}_i(0) = \boldsymbol{\mu}_{i0} \end{cases} \tag{14}$$

where $k_{bi} = E_i.I_i$ is the bending stiffness of the rod and r_{ci} the pre-curvature radius at rest. The rods have a rectangular cross section of dimensions h and w and for the sake of simplicity, we consider that $k_{b1} = k_{b2}$ and $r_{c1} = -r_{c2}$. The rest of geometric parameters are given in Table 1.

As explained in section 2.1, in the case of the inverse problem, the model of the robot's static configuration can be found by canceling the following residual:

$$\boldsymbol{\mathcal{R}}(\boldsymbol{y}, \boldsymbol{\rho}) = \begin{bmatrix} \boldsymbol{f}_{\text{P}} - \boldsymbol{n}_1(l_1) - \boldsymbol{n}_2(l_2) \\ m_{x,1}(l_1) \\ m_{x,2}(l_2) \\ \boldsymbol{p}_{\text{P}} - \boldsymbol{p}_1(l_1) + \boldsymbol{R}_1(0)\boldsymbol{a}_1 - \boldsymbol{R}_1(l_1)\boldsymbol{b}_1 \\ \boldsymbol{p}_{\text{P}} - \boldsymbol{p}_2(l_2) + \boldsymbol{R}_2(0)\boldsymbol{a}_2 - \boldsymbol{R}_2(l_2)\boldsymbol{b}_2 \\ \boldsymbol{p}_{\text{P}} - \boldsymbol{p}_{\text{des}} \end{bmatrix} = \boldsymbol{0} \tag{15}$$

where the state vector of the system $\boldsymbol{y} = [\boldsymbol{q}_a, \boldsymbol{p}_{\text{P}}, \boldsymbol{\mu}]^T \in \mathbb{R}^{10}$ is composed of the motor angles at the base of the rods ($\boldsymbol{q}_a \in \mathbb{R}^2$), the position of the EE platform ($\boldsymbol{p}_{\text{P}} \in \mathbb{R}^2$), and the ground wrenches of each leg ($\boldsymbol{\mu} \in \mathbb{R}^6$). The quantities $\boldsymbol{n}_i, m_{xi}$ and $\boldsymbol{p}_i$ are computed by forward integration of (14), $\boldsymbol{R}_i(s_i) \in \text{SO}(2)$ are the 2D rotation matrices of the legs, and $\boldsymbol{a}_i$ and $\boldsymbol{b}_i$ are the vectors representing the rigid segments of the mechanism. Finally, $\boldsymbol{f}_{\text{P}}$ denotes the external force applied at the EE and $\boldsymbol{p}_{\text{des}}$ corresponds to a desired position of the EE, imposed by the user or the environment.

Following the method presented in Section 2.2, we choose the bending stiffness and pre-curvature radius of each leg for the model parameters vector: $\boldsymbol{\rho} = [k_{b1}, r_{c1}, k_{b2}, r_{c2}]^T \in \mathbb{R}^4$. Other parameters such as the length of the legs and the rigid segments could also be studied, but here they are considered constant. The state sensitivity of each leg is then computed by applying the model in Equation (14) to Equation (8). The resulting matrices $\boldsymbol{\Pi}_1$ and $\boldsymbol{\Pi}_2$ are then used to compute the analytical expression of the Jacobian matrix $\frac{\partial \boldsymbol{\mathcal{R}}}{\partial \boldsymbol{\rho}}$. Finally, the full state sensitivity matrix of the robot $\boldsymbol{\Pi}_y$ is computed using Equation (9). In this paper we are interested in studying the behavior

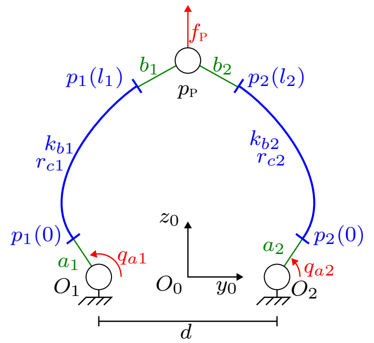

Fig. 1 R̲FRFR̲ robot parametrization

Table 1 Simulation parameters

Symbol	Value	Unit
l_i	250	mm
a_i	45	mm
b_i	35	mm
d	200	mm
w	2	mm
h	10	mm
f_P	[0,1]	N
k_{bi}	1.83e^{-2}	N.mm^2
r_{c1}	-1000	mm
δk_{bi}	4.73e^{-3}	N.mm^2
δr_{ci}	100	mm

of the EE position, thus we define a reduced state $\boldsymbol{y}_r = \boldsymbol{p}_P$ whose sensitivity matrix $\boldsymbol{\Pi}_{y_r}$ is:

$$\boldsymbol{\Pi}_{y_r} = \frac{\partial \boldsymbol{y}_r}{\partial \boldsymbol{\rho}} = \boldsymbol{\mathcal{S}}\boldsymbol{\Pi}_y \tag{16}$$

with $\boldsymbol{\mathcal{S}} \in \mathbb{R}^{n_{y_r} \times n_y}$ a selection matrix, that allows us to extract the elements of matrix $\boldsymbol{\Pi}_y$ that correspond to the reduced state. As such the reduced state sensitivity kernel matrix is:

$$\boldsymbol{K}_{\boldsymbol{\Pi}_{y_r}} = \boldsymbol{\mathcal{S}}\boldsymbol{K}_{\boldsymbol{\Pi}_y}\boldsymbol{\mathcal{S}}^T \tag{17}$$

In order to visualize the uncertainty ellipsoid described in Equation (13), we take the singular value decomposition of the kernel sensitivity matrix, i.e. $\boldsymbol{K}_{\boldsymbol{\Pi}_{y_r}} = \boldsymbol{U}\boldsymbol{\Sigma}\boldsymbol{V}^T$. Then we use the $\boldsymbol{U}$ and $\boldsymbol{V}$ matrices to transform a unit circle centered at the EE position, thus obtaining an ellipsoid in the yz-plane centered at the point $\boldsymbol{p}_p$ with semi-axes of length $\sqrt{\boldsymbol{\Sigma}}$.

To verify the validity of the presented method we select four points inside the robot's workspace (points A to D in Figure 2), for which we solve the robot model with nominal parameters and compute the uncertainty ellipsoids described in (13). Then, we simulate 2000 perturbed configurations, for which each parameter in $\boldsymbol{\rho}$ is chosen following a Gaussian law centered at the nominal value ρ^*_{ij}, and with a standard deviation $\sigma_{\rho_{ij}} = \delta\rho_{ij}/3$. The resulting perturbed parameters will lie inside the interval described in (6) in 99.7 % of cases according to the 3σ rule. As shown in Figure 2, the percentage of perturbed positions that lie within the ellipsoid surpasses 97 %, with the exception of point D. As shown by the size of the ellipsoid, point D is located in a high sensitivity zone. Furthermore, we can observe that the uncertainty ellipsoids are consistently stretched along one direction. In our case, this is explained by the fact that the largest eigen value in matrix $\boldsymbol{K}_{\boldsymbol{\Pi}_{y_r}}$ is always the one associated to the bending stiffness of the flexible segments,

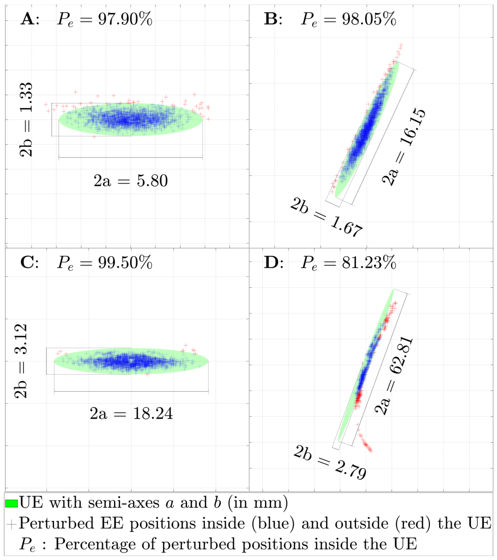

Fig. 2 Uncertainty Ellipsoids (UE) in different workspace locations

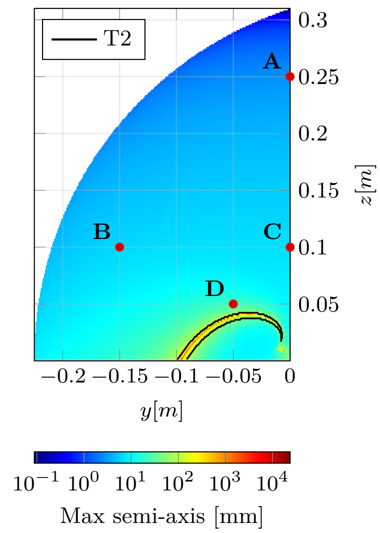

Fig. 3 Sensitivity analysis of half of the robot's workspace

thus showing that the CPR is more sensitive to variations of the bending stiffness of its legs than variations of their pre-curvature radius.

In order to evaluate the EE sensitivity across the workspace, we compute the largest uncertainty ellipsoid semi-axes in a discretized portion of the robot's workspace, as seen on Figure 3. Note that, using the simulation parameters of Table 1, the robot's workspace is symmetric relative to the z-axis. The lowest sensitivity values are obtained at the edge of the workspace while the high sensitivity values form a ring near the center of the base. Therefore, in the majority of the workspace, the ellipsoids presented in Figure 2 accurately encapsulate the clouds of perturbed EE positions. These results could be used to plan a trajectory passing through low sensitivity zones, in which the robot will be inherently more robust to parametric uncertainty. Additionally, the high sensitivity zones of Figure 3 seem to match the zones where Type 2 singularities arise which are delimited by the $T2$ line. These singularities are computed by following the method presented in [4], and correspond to configurations where a small displacement of the motors leads to a large displacement of the EE, separating the workspace between zones of stable and unstable robot configuration.

4 Conclusion

In this paper we provide a quantitative metric that links the impact of parametric uncertainty in the robot model, to the position of its end-effector. The method has been validated through simulations, and allows us to identify high and low sensitivity zones in the robot's workspace.

A notable limitation of the method is the fact that a preliminary testing campaign must be performed to find the variation range of the parameters. Additionally, the parameters should not deviate too much from their nominal value as the use of a first order approximation would no longer be valid.

Future perspectives include increasing the numbers of parameters in the model, generalizing the method to the 3D case and make use of this sensitivity metric for design optimization and trajectory planning.

Acknowledgements This work has been supported by the Agence Nationale de la Recherche under the France 2030 program, reference PEPR O2R-AS1 (ANR- 22-EXOD-0005)

References

1. Afifi, A., Belvedere, T., Pupa, A., Robuffo Giordano, P., Franchi, A.: Safe and Robust Planning for Uncertain Robots: A Closed-Loop State Sensitivity Approach. IEEE Robotics and Automation Letters **9**(11), 9962–9969 (2024)
2. Altuzarra, O., Caballero, D., Campa, F.J., Pinto, C.: Forward and Inverse Kinematics in 2-DOF Planar Parallel Continuum Manipulators. In: B. Corves, P. Wenger, M. Hüsing (eds.) EuCoMeS 2018, vol. 59, pp. 231–238. Springer International Publishing, Cham (2019)
3. Black, C.B., Till, J., Rucker, D.C.: Parallel Continuum Robots: Modeling, Analysis, and Actuation-Based Force Sensing. IEEE Transactions on Robotics **34**(1), 29–47 (2018)
4. Briot, S., Goldsztejn, A.: Singularity Conditions for Continuum Parallel Robots. IEEE Transactions on Robotics **38**(1), 507–525 (2022)
5. Case, J.C., White, E.L., Kramer, R.K.: Soft Material Characterization for Robotic Applications. Soft Robotics **2**(2), 80–87 (2015)
6. Srour, A.: Planification robuste pour systèmes robotiques. Ph.D. thesis, Université de Rennes (2024)
7. Stella, F., Pei, G., Meebed, O., Guan, Q., Bing, Z., Santina, C.D., Hughes, J.: Toward Long-Lasting Large-Scale Soft Robots: The Durability Challenge in Architectured Materials. In: 2024 IEEE 7th International Conference on Soft Robotics (RoboSoft), pp. 190–196 (2024)
8. Till, J., Rucker, D.C.: Elastic Stability of Cosserat Rods and Parallel Continuum Robots. IEEE Transactions on Robotics **33**(3), 718–733 (2017)
9. Wallin, T.J., Pikul, J., Shepherd, R.F.: 3D printing of soft robotic systems. Nature Reviews Materials **3**(6), 84–100 (2018)